

A Water Solvation Shell Can Transform Gold Metastable Nanoparticles in the Fluxional Regime

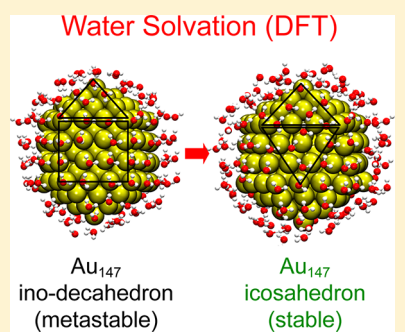
Chen-Hui Chan,[†] Floriane Poignant,[‡] Michaël Beuve,[‡] Elise Dumont,[†] and David Loffreda*,[†]

[†]Univ Lyon, Ens de Lyon, CNRS UMR 5182, Université Claude Bernard Lyon 1, Laboratoire de Chimie, F-69342 Lyon, France

[‡]Univ Lyon, Université Lyon 1, UMR CNRS5822/IN2P3, IPNL, PRISME, PHABIO, Villeurbanne 69322, France

Supporting Information

ABSTRACT: Solvated gold nanoparticles have been modeled in the fluxional regime by density functional theory including dispersion forces for an extensive set of conventional morphologies. The study of isolated adsorption of one water molecule shows that the most stable adsorption forms are similar (corners and edges) regardless of the nanoparticle shape and size, although the adsorption strength differs significantly (0.15 eV). When a complete and explicit water solvation shell interacts with gold nanoclusters, metastable in vacuum and presenting a predominance of (100) square facets (ino-decahedra Au₅₅ and Au₁₄₇), these nanoparticles are found unstable and transform into the closest morphologies exhibiting mainly (111) triangular facets and symmetries. The corresponding adsorption strength per water molecule becomes independent of shape and size and is enhanced by the formation of two hydrogen bonds on average. For applications in radiotherapy, this study suggests that the shapes of small gold nanoparticles should be homogenized by interacting with the biological environment.



Functionalized gold nanoparticles (NPs) have been considered in recent years as promising materials for applications in biomedicine, especially for radiotherapy and cancer treatment.^{1–5} Their excellent biocompatibility, long blood circulation time, and the possibility of their functionalization make them highly desirable for theranostics. In fact, they contribute to radiosensitization effects, making tumor cells more responsive to ionizing radiation.^{6,7} Under irradiation, Au NPs in water generate more electrons and reactive oxygen species, which may amplify the damage caused by radiation.^{7,8} To date, although the structure of gold nanoparticles has been examined in model conditions by diffraction and microscopic measurements,^{9–14} little is known at the atomic scale regarding the morphology, structure, and energetics of Au NPs in contact with liquid water (biological natural environment).

The lack of information and understanding opens the way to theoretical modeling. Indeed, typical Au NP working sizes are in the range of 30–50 nm.^{1,3} However, smaller Au NPs (1.9 nm) are proposed in the context of radiotherapy enhancement,^{15,16} although monodisperse ultrasmall NPs are difficult to synthesize. Hence, theoretical simulations of Au NPs approaching this range can result in an interesting understanding. For instance, interfacial chemical and physical processes happening at the vicinity of functionalized Au NPs can be explored by atomistic calculations while water radiolysis can be studied by continuous models and Monte Carlo simulations like LiQuiD code.^{17,18} These two complementary approaches may provide a better understanding of interfacial properties while Monte Carlo simulations may benefit from useful atomistic information. Concerning the modeling of the

interface between Au NPs and water solvation at the atomic scale, density functional theory (DFT) is a powerful tool to predict optimal geometries and energetics. In DFT studies, static approaches are often considered to describe water adsorption on Au surfaces^{19–24} and nanoclusters up to 20 atoms,²⁵ although the explicit interface between metallic nanoparticles and liquid water can be described by ab initio molecular dynamics simulations.²⁶ To date, a few studies based on parametrized force fields and classical molecular dynamics simulations have been reported in the literature for gold/water interfaces.^{27,28,23} Regarding the question of Au NPs' most likely morphologies and shapes as a function of size and temperature, a few investigations have been proposed on the basis of either Au NPs modeled in vacuum by explicit 3D structures^{29–34} or Au NPs in a water vapor environment described by extended metallic surfaces calculated by DFT and Wulff construction for predicting thermal properties.³⁵ According to a recent DFT study,³² Au NPs in vacuum can exist in various shapes at different sizes in the fluxional regime (1–3.5 nm), with a preference for icosahedral morphology (decahedral and octahedral ones being metastable). Global optimization methods based on semiempirical potentials have shown the versatility of gold shapes in the fluxional regime (below 100 atoms).^{29,30} At a larger scale (1000 atoms), these approaches show that truncated octahedra and Marks-decahedra are in competition, whereas icosahedra are the least stable NPs.^{31,36–38} In addition, cuboctahedra and ino-

Received: December 21, 2018

Accepted: February 1, 2019

Published: February 1, 2019

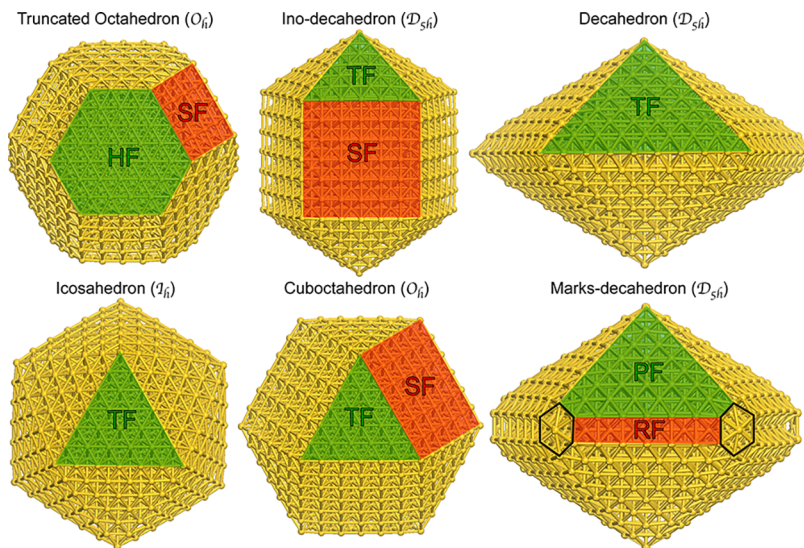


Figure 1. Definition of the considered Au NP morphologies in the range of 0.9–3.4 nm (44 NPs). Truncated octahedra (to), cuboctahedra (cubo), ico-decahedra (ino), and Marks decahedra (marks) are composed of mixed facets [hexagonal (HF), triangular (TF), and pentagonal (PF) with square (SF) or rectangular (RF) facets], whereas decahedra (deca) and icosahedra (ico) present only triangular facets (TF).

decahedra become more stable than icosahedra³¹ in contrast with a recent DFT study of large NP size.³² A water monomer on small gold nanoclusters (less than 20 atoms) mainly interacts with gold at corner adsorption sites with a variable stability, depending also on the choice of the DFT functional (0.2–0.4 eV with vdW-DF and 0.25–0.5 eV with PBE).²⁵ This stability is larger than the adsorption energy calculated on Au(111) (−0.105/−0.14 eV with PW91,^{19,20} −0.11 eV with PBE,^{21,22} −0.24 eV with PBE-D2,²¹ −0.30 eV with optB86b-vdW,²¹ and −0.192 eV with revPBE-vdW²²). The water vapor effect on Au nanoparticle shape is rather small by comparison with other metals and consists of a progressive transformation of (100) facets in favor of (111) ones becoming larger in truncated octahedra.³⁵

Hence, an explicit static or dynamic atomistic model describing the interaction of water monomers and solvation shells (in particular first solvation shell around the nanoparticle) with gold nanoparticles in the range 1–2 nm is still missing. In this work, we develop DFT models of water adsorption on a family of several convex and regular gold polyhedra (including octahedral and icosahedral shapes) and of water solvated Au NPs with a static approach including dispersion forces. We aim to probe the water effect on Au NPs' morphology and size as a first model describing the influence of the biological environment. In particular, we examine, in a comprehensive and systematic study, the adsorption energetics for water, especially for decahedral gold shapes, a competitive form which has been rarely considered in the theoretical literature at the DFT level to date.

The first step is the determination of competitive morphologies in the range of sizes accessible by DFT calculations. In Figure 1, the polyhedra considered in this study are defined, including the three key octahedral, icosahedral, and decahedral symmetries according to the literature^{36,37} (see Figures S1–S6 for all the optimal structures of the considered 44 NPs). The question of the most stable morphology according to the size of the NP is a debate.^{31,32,36–38} In this work, we address this question by DFT calculations including dispersion forces. Figure 2a plots the cohesion energy of the NP in vacuum against $N^{-1/3}$ (see eq

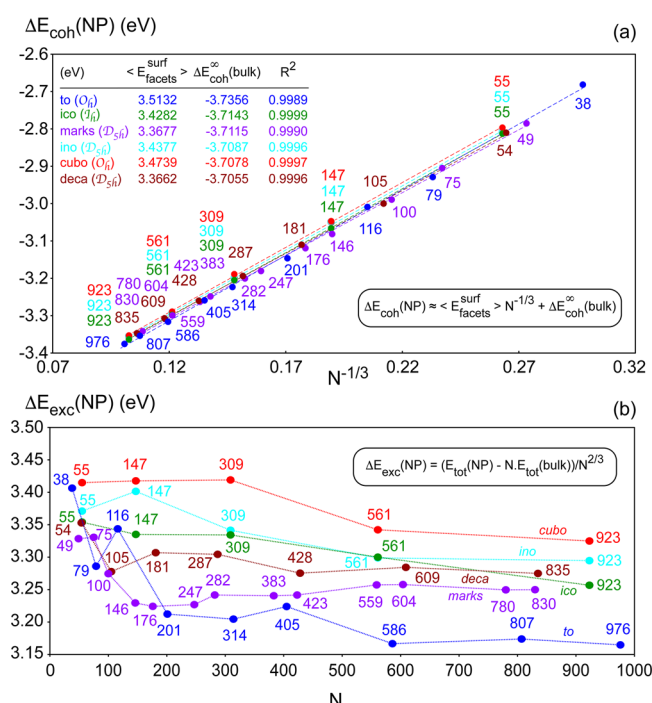


Figure 2. (a) Normalized cohesion energy per atom $\Delta E_{\text{coh}}(\text{NP})$ (eV) diagram against $N^{-1/3}$, where N is the number of Au atoms in the NP. The parameters (slope, offset, and R^2) of the linear regressions are defined in the equation, where the slope $\langle E_{\text{facets}}^{\text{surf}} \rangle$ (eV) can be identified as the average facet surface energy of the NP (including center, edge, and corner atoms) and the offset $\Delta E_{\text{coh}}^{\infty}(\text{bulk})$ (eV) as the cohesion energy extrapolated for the bulk (infinite value of N). The six different families of the NPs are reported with different colors defined in the inset where the parameters of the linear regression for each shape family are exposed (the stability for each family being captured in average by the values of the offsets). (b) Excess energy $\Delta E_{\text{exc}}(\text{NP})$ (eV) diagram against the number N of Au atoms in the NP according to the defined formula.

S1 in the Supporting Information). For each polyhedral family among the six key shapes exposed in Figure 1, we have quantified the slopes and the offsets of the linear laws obtained

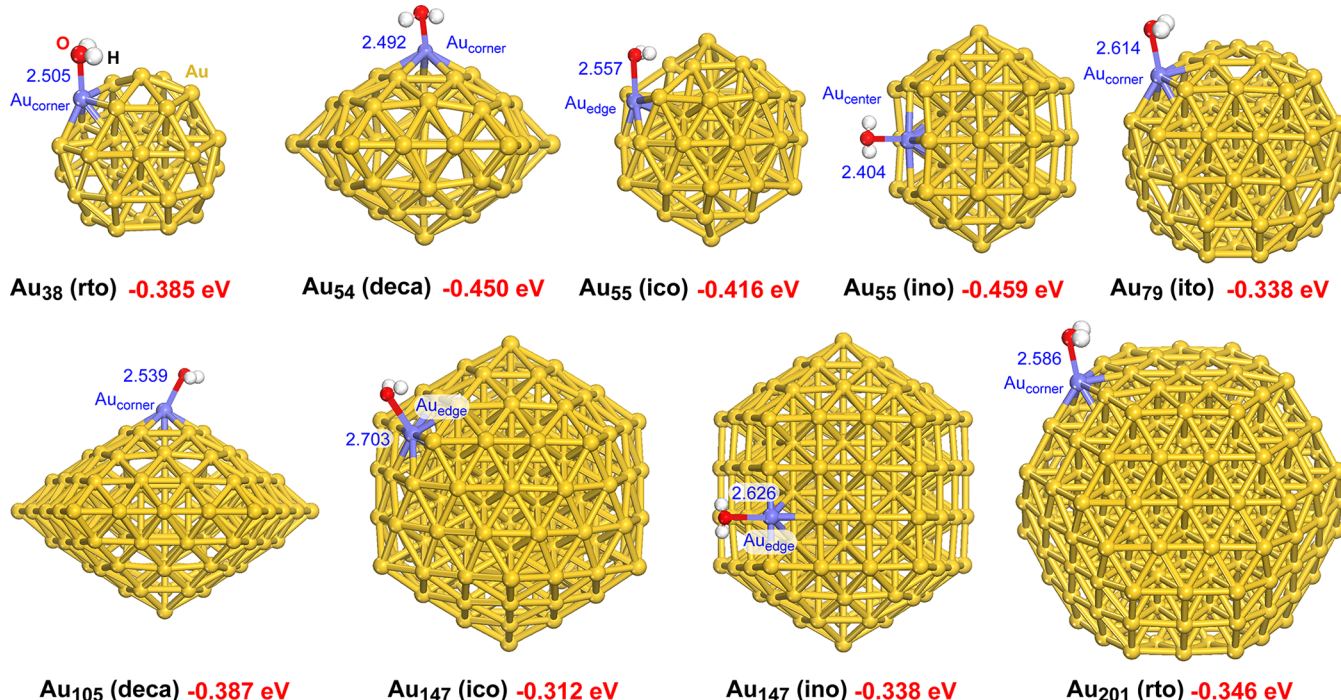


Figure 3. Optimized adsorption structures of a water monomer on nine different Au NPs in the range 0.9–1.8 nm, including four competitive morphologies: regular and irregular truncated octahedron (rto and ito, respectively), icosahedron (ico), ino-decahedron (ino), and decahedron (deca). The definitions of colors for atoms are given, as well as the location of the surface Au adsorption site with the following possibilities: corner, edge, and facet center. The Au–O bond distances are reported in Å (blue), whereas the adsorption energies in are given in eV (red).

in the range 0.9–3.4 nm (38–976 atoms). In addition, we propose to compare the trends coming from the cohesion energy with those resulting from the calculation of excess energy (normalized by $N^{-2/3}$; see eq S2 in the Supporting Information), as displayed in Figure 2b, a relevant descriptor which separates more clearly the nanoparticle stability.^{36,37} In Figure 2a, the linear laws for the cohesion energy show that two terms are in competition for the NP stability: the offset corresponding to the cohesion energy in the Au bulk and the slope related to the average facets surface energy including facet, edge and corner atoms. The obtained offsets are close to the calculated bulk cohesion energy (-3.695 eV/atom) in good agreement with experiment (-3.81 eV/atom). Our linear models are in better agreement with experiments of previous DFT work³² (-3.285 eV for the icosahedra with the TPSS functional). However, they differ slightly from one polyhedral family to another because the examined range of NP size is limited (below 3.4 nm). The truncated octahedral NPs have the most stable offset (-3.736 eV/atom). They compete with icosahedra and Marks-decahedra with bulk cohesion energy of -3.714 and -3.711 eV/atom, respectively. In contrast, the decahedral NPs (regular and Marks) show the minimal facet surface energies (3.367 eV). This is expected because these polyhedra exhibit mainly large (111)-facet type. Then comes the icosahedra with small (111)-facet type (3.428 eV in this work, whereas 2.478 eV was proposed previously³²). The NPs having the highest average facet surface energy are truncated octahedra, ino-decahedra, and cuboctahedra because they possess large (100)-facet type, well-known to be less stable than the (111) type. To clarify this picture, we have examined the NP relative stability with the excess energy. In Figure 2b, the calculations show that two shapes compete in the range of 0.9–1.8 nm: truncated octahedral and decahedral (regular and Marks); the Au₅₅ icosahedron is also competitive. Above 1.8

nm (201 atoms), the truncated octahedra become really more stable than the other polyhedra. At 3.4 nm (about 1000 atoms), they predominate while the Marks-decahedra and icosahedra are minority. Our picture differs from previous systematic studies based on global optimization methods, effective semiempirical potentials, and Monte Carlo simulations concluding that decahedral shapes are either majority or equivalent in stability to truncated octahedral forms.^{36,37,31,38} In addition, the stability of icosahedra tends to slightly increase with the NP size, in contrast with these previous studies. Our global trends are in better agreement with a previous study based on simulations obtained with the Sutton–Chen potential,³⁹ and they also support in part the recent DFT study examining a set of Au NPs with the TPSS functional.³² Several experimental studies based on HAADF-STEM measurements have been reported for the determination of the structure of gold nanoclusters, especially for particular sizes 309,¹² 561,¹³ and 923 atoms.¹⁴ The reported images in these publications show the preference of defective decahedral and face-centered cubic forms with respect to icosahedral shape. Our DFT results support these conclusions because truncated octahedral and Marks-decahedral forms are found more stable than the icosahedral shape above 300 atoms.

On the basis of this study, we examined the adsorption properties of a water monomer on the most competitive polyhedra in the range 0.9–1.8 nm, as shown in Figure 3. The truncated octahedra Au₃₈, Au₇₉, and Au₂₀₁ have been selected, as well as decahedra Au₅₄ and Au₁₀₅. In addition, metastable shapes such as icosahedra and ino-decahedra have also been considered to explore the impact of water adsorption on their metastability. Because of the complexity of the water solvation shell examined later, the largest considered cluster is Au₂₀₁. In Figure 3, for each of the 9 nanoclusters, the most stable adsorption structures have been reported [including adsorp-

tion energetics (see eq S3 in the Supporting Information), Au–O distance, and site], while all the metastable adsorption forms are presented in Figures S7–S15. Moreover, the decomposition of adsorption energetics in covalence and dispersion contributions are provided in Table S1. As the size of the NP increases, the adsorption site changes (although the adsorption at a corner remains the majority) and the evolution of the adsorption energy is not monotonous, with values in a narrow range: from -0.31 to -0.46 eV. Our results agree with previous DFT values proposed on Au small clusters²⁵ and Au(111).^{21,22} The adsorption of a water molecule is thus a weak chemisorption with a quite long Au–O distance in the range of 2.40 – 2.63 Å. This is consistent with the weak deformation of Au NPs after adsorption. To quantify this, an energy decomposition analysis of adsorption energetics is proposed in Figure 4. According to this analysis, the

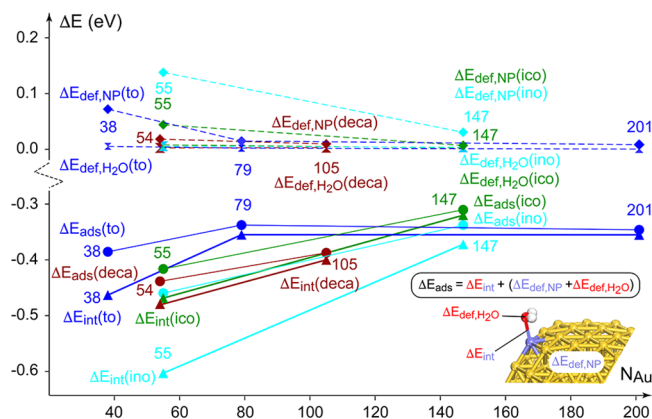


Figure 4. Energy diagram against the number of Au atoms in the NPs, showing the energy decomposition analysis (EDA) of the adsorption energy (ΔE_{ads} , eV) of water monomer on nine different Au clusters with four different shapes (defined by specific colors) in the range 0.9–1.8 nm (see Figure 2 for the optimal adsorption structures). ΔE_{ads} is expressed in the equation as the sum of the pure binding energy between Au NP and water (ΔE_{int} , energy gain), the deformation energy of water between optimal isolated situation and the geometry in the adsorption form ($\Delta E_{\text{def}, \text{H}_2\text{O}}$, energy cost), and the equivalent deformation energy of Au NP ($\Delta E_{\text{def}, \text{NP}}$, energy cost).

deformation energy of the Au NPs is positive and weak in general for all the shapes in the 0.01–0.14 eV range. In parallel, the deformation energy of the water monomer is also positive and close to zero (below 8 meV). This means that the nonmonotonous trend of adsorption energy is mainly captured by the interaction energy between the Au cluster and water. Moreover, this interaction, which corresponds to the chemical bonding between both partners, is the strongest one (-0.6 eV) for the ino-decahedral NPs and for the icosahedral shape at least for a small size (-0.47 eV). For the most stable NPs (truncated octahedra and decahedra), the chemical bonding is quite weaker (from -0.32 to -0.47 eV) and it varies less with the cluster size.

On the basis of the best adsorption structures of water monomers on the Au NPs, we then propose to explore the interaction of a complete shell of water molecules around the metallic clusters by a static approach. The starting geometries of these solvation shells come from an additive principle assuming that the coadsorption of the best sites is an optimal choice for maximizing the overall stability of the solvated nanocluster. This means that, for the various NPs, all the

equivalent sites corresponding to the best adsorption form of monomers are occupied by water molecules. Then, to complete the solvation shells, metastable adsorption sites were considered in such a way that a network of flat co-physisorbed and co-chemisorbed water molecules is built up through hydrogen bonds with reasonable distances (longer than 1.8 Å). Thus, because all the molecules were initially coplanar with respect to one facet, no arbitrary choice related to H-up/H-down configuration has been considered by construction. This starting choice was also guided by a previous molecular dynamics study of immersed Au clusters (13, 55, and 147) in water, showing that the hydrogen bonding of water molecules is arranged in a two-dimensional structure for Au_{55} and Au_{147} .²⁸ The final structures of the solvation shells obtained after geometry optimizations are reported in Figure 5. Details of the total number of water molecules per NP; the numbers of chemisorbed and physisorbed molecules; and analyses of adsorption energetics, nanoparticle structural deformation induced by water monoshells, and hydrogen bonds are given in Tables S2 and S3 and Figure S17. The surface coverage of water is addressed in Figure 5, with the ratio of chemisorbed and physisorbed molecules. When the size of the NP increases, this coverage decreases in average progressively from 0.44 to 0.23 ML with two exceptions at sizes 55 and 147 for icosahedral (0.40 ML) and ino-decahedral (0.31 ML) shapes. In a concomitant way, the number of chemisorbed molecules decreases in favor of physisorbed water (the ratio decreasing in average from 0.27 to 0.15), again with two exceptions for Au_{55} (0.28) and Au_{147} (0.22). At the largest size (Au_{201}), the calculated coverage of 0.23 ML is smaller than the one proposed previously (0.29 ML) for an explicit liquid water/Pt₂₀₁ interface investigated by ab initio molecular dynamics at 350 K.²⁶ Our result for Au with a static approach is thus reasonable because the chemical bonding on Au_{201} (-0.35 eV) is almost twice weaker than the one found on Pt₂₀₁ (-0.54 eV). For the two exceptions of larger coverage of chemisorbed water on Au_{55} and Au_{147} (icosahedra and ino-decahedra), this is only a direct consequence of the stronger interaction energy or chemical bonding discussed before, not the fact that these clusters would present more stable adsorption sites in number.

At first glance, these optimal structures are relatively homogeneous regarding the distribution of chemisorbed and physisorbed water and as a function of the NP size; however, no clear arrangement appears, in agreement with a previous MD study.²⁸ In addition, the solvation shells are quite spherical around the Au NPs, thus meaning that the average interaction between each water molecule and the cluster should not vary much. This can be seen with the average adsorption energy per water (from -0.607 to -0.643 eV/water), which does not change much against the nanocluster size (see eq S4 in the Supporting Information). This contrasts with the adsorption of the monomer discussed before. The adsorption energy per water is in average 70% stronger for the solvation shell with respect to the isolated adsorption. According to the optimal geometries, this gain is certainly not due to a strengthening of chemisorbed water but rather to the formation of chemical bonds between the molecules (hydrogen bonds). In fact, on the basis of the energetic models presented in the Supporting Information (see eqs S7–S13, Table S3, and Figure S18), the adsorption energy per water of the solvation shell is mainly due to the formation of two hydrogen bonds in average (from -0.49 to -0.59 eV/water depending on the NP size), the rest

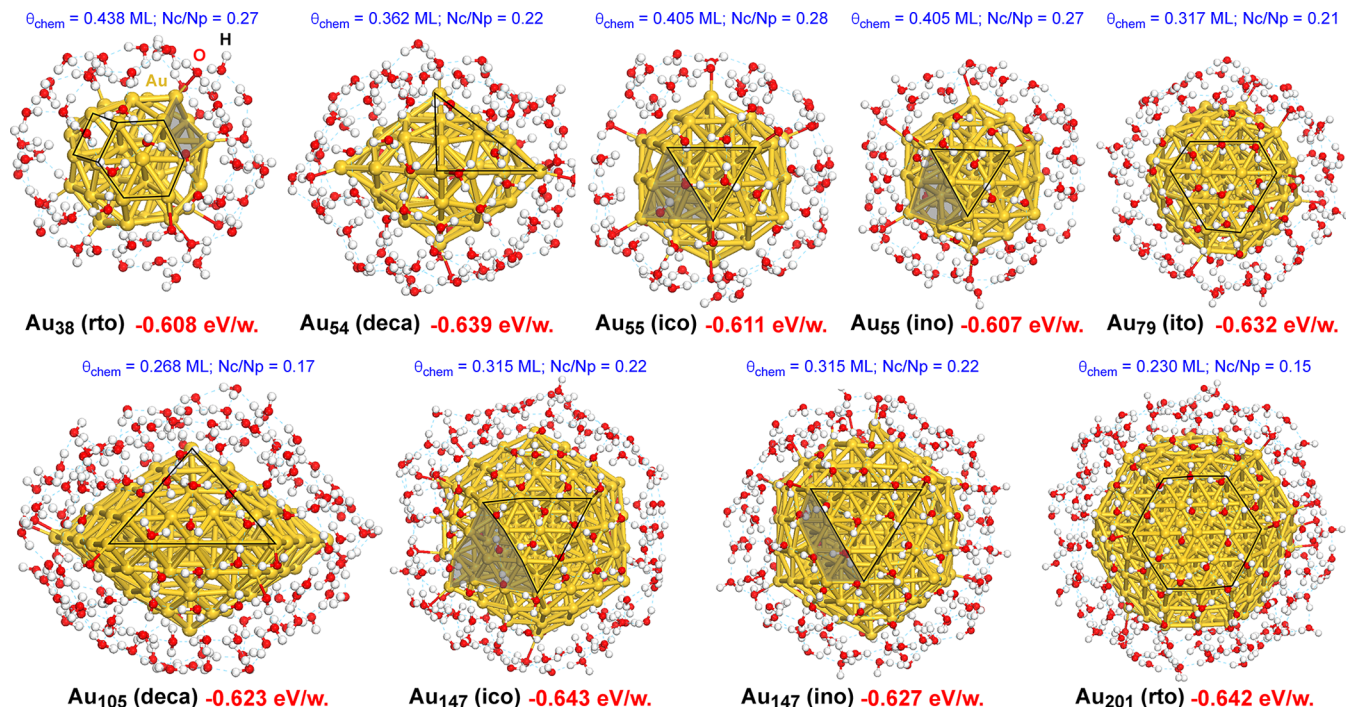


Figure 5. Optimized adsorption structures of a shell of water molecules on nine different Au NPs in the range 0.9–1.8 nm, including four competitive morphologies: regular and irregular truncated octahedron (rto and ito, respectively), icosahedron (ico), ino-decahedron (ino), and decahedron (deca). The definitions of colors for atoms are given. The adsorption energies in eV per water molecule in total are reported (red), as well as the surface coverage of chemisorbed water molecules in ML (monolayer) and the ratio N_c/N_p between chemisorbed water (N_c) and physisorbed water (N_p). The complex network of hydrogen bonds is also marked by light gray dotted lines. The strongly distorted facets of icosahedral (and transformed ino-decahedral) shapes are drawn with full gray areas for Au₅₅ and Au₁₄₇.

being the interaction energy between water and gold (around -0.1 eV/water). In the case of Au NPs, the formation of the water shell occurs at the detriment of chemisorption, because the latter is rather weak. Hence, for Au NPs in the 0.8–1.9 nm range, both the stability of the solvation shell (-0.6 eV/water) and the average number of formed hydrogen bonds (golden rule of 2) are remarkably independent of the NP size and morphology. By comparison, in bulk water, the cohesion energy per water molecule is known from experiments (-9.9 kcal/mol or -0.429 eV/water).⁴⁰ In addition, the two-body contribution of the dissociation energy of water dimers benchmarked by coupled cluster calculations on configurations extracted from ab initio molecular dynamics simulations of liquid water has been evaluated to be -0.137 eV (while it is -0.221 eV at equilibrium in the gas phase).⁴¹ This means that the maximum number of hydrogen bonds per water molecule in bulk liquid can be estimated to be 3.13 bonds, considering that only hydrogen bonding contributes to the cohesion energy in the liquid. This assumption agrees with previous experimental measurements from neutron diffraction⁴² (3.58 hydrogen bonds per water molecule) and with a Car-Parrinello molecular dynamics simulation study⁴³ (3.48 hydrogen bonds per water molecule). Hence, we found a decrease of the number of hydrogen bonds in our solvation shells (“onion peel”) around Au NPs (from 2.06 to 2.51 hydrogen bonds per water, see Table S3) by comparison with bulk water, in fair agreement with a previous MD study.²⁷

Considering now the impact of the water solvation shells on the geometry of the Au NPs after the geometry optimizations, deformations of the clusters are observed in Figure 5, even for the most stable case in vacuum, such as Au₃₈, Au₅₄, and Au₇₉. This impact is also seen for the less stable icosahedra Au₅₅ and

Au₁₄₇. A quantitative analysis of the structural deformation of the nanoparticle outershells upon water adsorption is addressed in the Supporting Information (see eqs S5–S6, Table S2, and Figure S17). Moreover, the metastable ino-decahedra Au₅₅ and Au₁₄₇ in vacuum are transformed into corresponding icosahedra through the interaction with the water shells. This original result is counterintuitive because water chemisorption on Au is quite weak as reported before, and HAADF-STEM images show that gold icosahedral nanoclusters in model operating conditions (in the range 1–3 nm) transform into decahedral structures.^{12–14} However, the increase of the chemical bond with water obtained for these clusters and the concomitant increase of chemisorbed water coverage discussed previously allow us to explain the origins of such a remarkable phenomenon. Then in this study we demonstrate that water, standing for a model of the biological environment, may have a significant impact on the morphology of metastable NP shapes, although the intrinsic interaction with water is relatively weak.

Our DFT work opens promising perspectives for a reparametrization of semiempirical potentials and global optimization methods aiming to describe the relative stability between ino-decahedra and icosahedra in interaction with a water solvation shell at larger NP size. In particular, this would allow the study of Au₃₀₉, Au₅₆₁, and Au₉₂₃, both with static and dynamic approaches for Au/water interfaces, and this would show whether the water solvation still induces the transformation between metastable morphologies at larger NP size.

■ COMPUTATIONAL METHODS

DFT calculations (spin restricted) of Au NPs and water adsorption were performed by using the VASP code, version

5.3.5.^{44–46} PBE⁴⁷ with Grimme's D3 semiempirical dispersion-corrected functional⁴⁸ (zero-damping formalism) was considered to describe electronic exchange and correlation at the generalized gradient approximation with van der Waals interactions. The core electrons were described by the projector-augmented wave⁴⁹ (PAW) pseudopotentials (11 valence electrons per Au atom), and valence electrons were expanded in plane waves with a kinetic cutoff energy of 400 eV. All the Au NPs were modeled in a cubic box of $5 \times 5 \times 5$ nm³ with a Γ -point only approach for the k-point mesh and related Brillouin zone. For the Au bulk, the fcc crystalline structure was described by using a k-point grid of $17 \times 17 \times 17$. In the geometry optimizations, the Au NPs and water adsorption structures were relaxed completely with 10^{-6} eV for the convergence of the total electronic energy and -0.01 eV·Å⁻¹ for the minimization of the residual forces on the nuclei. A Methfessel–Paxton smearing was used for the calculation of the total electronic energy.

■ ASSOCIATED CONTENT

Supporting Information

The Supporting Information is available free of charge on the ACS Publications website at DOI: [10.1021/acs.jpcllett.8b03822](https://doi.org/10.1021/acs.jpcllett.8b03822).

Definitions of Au NP cohesion energy, excess energy, and adsorption energy for water monomers and monoshells; (Figures S1–S6) complete set of optimized structures of free Au NPs; (Figures S7–S15) complete set of optimized adsorption structures of water monomers on 9 Au NPs in the range of 0.9–1.8 nm (adsorption sites and energies, Au–O distances); (Figure S16) adsorption energy decomposition model in covalence and dispersion for water monomers on Au NPs in the range of 0.9–1.8 nm; (Table S1) adsorption energy decomposition model in covalence and dispersion for water monoshells on Au NPs in the range 0.9–1.8 nm; (Equations S1–S13) definitions of excess energy, cohesion energy for free Au NPs, adsorption energy for water, hydrogen bonding model, and roundness degree; (Table S2 and Figure S17) geometric analysis of the nanoparticle deformation upon water adsorption based on the variation of the roundness degree; (Table S3 and Figure S18) hydrogen bonding model for water shells on Au NPs ([PDF](#))

■ AUTHOR INFORMATION

Corresponding Author

*E-mail: david.loffreda@ens-lyon.fr.

ORCID

David Loffreda: [0000-0001-9912-7965](https://orcid.org/0000-0001-9912-7965)

Notes

The authors declare no competing financial interest.

■ ACKNOWLEDGMENTS

The authors thank Dr. Christine Mottet (CiNAM, Marseille, France) for helpful discussions. They also thank IDRIS in Paris, CINES in Montpellier, TGCC in Grenoble (project 609, GENCI/CT8), and PSMN in Lyon for CPU time and assistance. C.-H.C. and F.P. thank LABEX PRIMES (ANR-11-LABX-0063) of Université de Lyon (within the program “Investissements d’Avenir” ANR-11-IDEX-0007) for Ph.D.

funding. F.P. thanks “Fondation ARC pour la recherche sur le cancer” for support. The authors thank the SYSPROD project and AXELERA Pôle de Compétitivité for financial support (PSMN Data Center).

■ REFERENCES

- (1) Laprise-Pelletier, M.; Simao, T.; Fortin, M.-A. Gold nanoparticles in radiotherapy and recent progress in nanobrachytherapy. *Adv. Healthcare Mater.* **2018**, *7*, 1701460.
- (2) Henderson, L.; Neumann, O.; Kaffes, C.; Zhang, R.; Marangoni, V.; Ravoori, M. K.; Kundra, V.; Bankson, J.; Nordlander, P.; Halas, N. J. Routes to potentially safer T1 magnetic resonance imaging contrast in a compact plasmonic nanoparticle with enhanced fluorescence. *ACS Nano* **2018**, *12* (8), 8214–8223.
- (3) Gilles, M.; Brun, E.; Sicard-Roselli, C. Gold nanoparticles functionalization notably decreases radiosensitization through hydroxyl radical production under ionizing radiation. *Colloids Surf., B* **2014**, *123*, 770–777.
- (4) Brun, E.; Sicard-Roselli, C. Actual questions raised by nanoparticle radiosensitization. *Radiat. Phys. Chem.* **2016**, *128*, 134–142.
- (5) Her, S.; Jaffray, D. A.; Allen, C. Gold nanoparticles for applications in cancer radiotherapy: Mechanisms and recent advancements. *Adv. Drug Delivery Rev.* **2017**, *109*, 84–101.
- (6) Kobayashi, K.; Usami, N.; Porcel, E.; Lacombe, S.; Le Sech, C. Enhancement of radiation effect by heavy elements. *Mutat. Res., Rev. Mutat. Res.* **2010**, *704* (1–3), 123–131.
- (7) Peukert, D.; Kempson, I.; Douglass, M.; Bezak, E. Metallic nanoparticle radiosensitisation of ion radiotherapy: a review. *Physica Medica* **2018**, *47*, 121–128.
- (8) Vankayala, R.; Kuo, C.-L.; Nuthalapati, K.; Chiang, C.-S.; Hwang, K.-C. Nucleus-Targeting Gold Nanoclusters for Simultaneous In Vivo Fluorescence Imaging, Gene Delivery, and NIR-Light Activated Photodynamic Therapy. *Adv. Funct. Mater.* **2015**, *25*, 5934–5945.
- (9) Cleveland, C. L.; Landman, U.; Schaaff, T. G.; Shafiqullin, M. N.; Stephens, P. W.; Whetten, R. L. Structural Evolution of Smaller Gold Nanocrystals: The Truncated Decahedral Motif. *Phys. Rev. Lett.* **1997**, *79*, 1873.
- (10) Koga, K.; Takeo, H.; Ikeda, T.; Ohshima, K.-I. In situ grazing-incidence x-ray-diffraction and electron-microscopic studies of small gold clusters. *Phys. Rev. B: Condens. Matter Mater. Phys.* **1998**, *57*, 4053.
- (11) Koga, K.; Ikeshoji, T.; Sugawara, K.-I. Size- and Temperature-Dependent Structural Transitions in Gold Nanoparticles. *Phys. Rev. Lett.* **2004**, *92*, 115507.
- (12) Li, Z. Y.; Young, N. P.; Di Vece, M.; Palomba, S.; Palmer, R. E.; Bleloch, A. L.; Curley, B. C.; Johnston, R. L.; Jiang, J.; Yuan, J. Three-dimensional atomic-scale structure of size-selected gold nanoclusters. *Nature* **2008**, *451*, 46–48.
- (13) Foster, D. M.; Ferrando, R.; Palmer, R. E. Experimental determination of the energy difference between competing isomers of deposited, size-selected gold nanoclusters. *Nat. Commun.* **2018**, *9*, 1323.
- (14) Plant, S. R.; Cao, L.; Palmer, R. E. Atomic Structure Control of Size-Selected Gold Nanoclusters during Formation. *J. Am. Chem. Soc.* **2014**, *136*, 7559–7562.
- (15) Butterworth, K. T.; Coulter, J. A.; Jain, S.; Forker, J.; McMahon, S. J.; Schettino, G.; Prise, K. M.; Currell, F. J.; Hirst, D. G. Evaluation of cytotoxicity and radiation enhancement using 1.9 nm gold particles: potential application for cancer therapy. *Nanotechnology* **2010**, *21* (29), 295101.
- (16) Jain, S.; Coulter, J. A.; Butterworth, K. T.; Hounsell, A. R.; McMahon, S. J.; Hyland, W. B.; Muir, M. F.; Dickson, G. R.; Prise, K. M.; Currell, F. J.; Hirst, D. G.; O’Sullivan, J. M. Gold nanoparticle cellular uptake, toxicity and radiosensitisation in hypoxic conditions. *Radiother. Oncol.* **2014**, *110* (2), 342–347.

- (17) Gervais, B.; Beuve, M.; Olivera, G. H.; Galassi, M. E.; Rivarola, R. D. Production of HO₂ and O₂ by multiple ionization in water radiolysis by swift carbon ions. *Chem. Phys. Lett.* **2005**, *410* (4–6), 330–334.
- (18) Gervais, B.; Beuve, M.; Olivera, G. H.; Galassi, M. E. Numerical simulation of multiple ionization and high LET effects in liquid water radiolysis. *Radiat. Phys. Chem.* **2006**, *75* (4), 493–513.
- (19) Meng, S.; Wang, E. G.; Gao, S. Water adsorption on metal surfaces: a general picture from density functional theory studies. *Phys. Rev. B: Condens. Matter Mater. Phys.* **2004**, *69*, 195404.
- (20) Phatak, A. A.; Delgass, W. N.; Ribeiro, F. H.; Schneider, W. F. Density functional theory comparison of water dissociation steps on Cu, Au, Ni, Pd and Pt. *J. Phys. Chem. C* **2009**, *113*, 7269–7276.
- (21) Nadler, R.; Sanz, J. F. Effect of dispersion correction on the Au (1 1 1)-H₂O interface: a first-principles study. *J. Chem. Phys.* **2012**, *137* (11), 114709.
- (22) Carrasco, J.; Klimes, J.; Michaelides, A. The role of van der Waals forces in water adsorption on metals. *J. Chem. Phys.* **2013**, *138*, 024708.
- (23) Berg, A.; Peter, C.; Johnston, K. Evaluation and Optimization of Interface Force Fields for Water on Gold Surfaces. *J. Chem. Theory Comput.* **2017**, *13* (11), 5610–5623.
- (24) Lin, X.; Groß, A. First-principles study of the water structure on flat and stepped gold surfaces. *Surf. Sci.* **2012**, *606*, 886–891.
- (25) Xue, Y. Water monomer interaction with gold nanoclusters from van der Waals density functional theory. *J. Chem. Phys.* **2012**, *136* (2), 024702.
- (26) de Morais, R. F.; Kerber, T.; Calle-Vallejo, F.; Sautet, P.; Loffreda, D. Capturing solvation effects at a liquid/nanoparticle interface by Ab Initio molecular dynamics: Pt201 immersed in water. *Small* **2016**, *12* (38), 5312–5319.
- (27) Ju, S.-P. A molecular dynamics simulation of the adsorption of water molecules surrounding an Au nanoparticle. *J. Chem. Phys.* **2005**, *122*, 094718.
- (28) Chang, C. I.; Lee, W. J.; Young, T. F.; Ju, S. P.; Chang, C. W.; Chen, H. L.; Chang, J. G. Adsorption mechanism of water molecules surrounding Au nanoparticles of different sizes. *J. Chem. Phys.* **2008**, *128* (15), 154703.
- (29) Häberlen, O. D.; Chung, S.-C.; Stener, M.; Rösch, N. From clusters to bulk: a relativistic density functional investigation on a series of gold clusters Au n, n = 6, ..., 147. *J. Chem. Phys.* **1997**, *106*, 5189–5201.
- (30) Ferrando, R.; Fortunelli, A.; Rossi, G. Quantum effects on the structure of pure and binary metallic nanoclusters. *Phys. Rev. B: Condens. Matter Mater. Phys.* **2005**, *72*, 085449.
- (31) Logsdail, A. J.; Li, Z. Y.; Johnston, R. L. Faceting preferences for AuN and PdN nanoclusters with high-symmetry motifs. *Phys. Chem. Chem. Phys.* **2013**, *15*, 8392–8400.
- (32) Li, H.; Li, L.; Pedersen, A.; Gao, Y.; Khetrapal, N.; Jónsson, H.; Zeng, X. C. Magic-number gold nanoclusters with diameters from 1 to 3.5 nm: Relative stability and catalytic activity for CO oxidation. *Nano Lett.* **2015**, *15* (1), 682–688.
- (33) Tarrat, N.; Rapacioli, M.; Cuny, J.; Morillo, J.; Heully, J.-L.; Spiegelman, F. Global optimization of neutral and charged 20- and 55-atom silver and gold clusters at the DFTB level. *Comput. Theor. Chem.* **2017**, *1107*, 102–114.
- (34) Tarrat, N.; Rapacioli, M.; Spiegelman, F. Au147 nanoparticles: ordered or amorphous? *J. Chem. Phys.* **2018**, *148*, 204308.
- (35) Zhu, B.; Xu, Z.; Wang, C.; Gao, Y. Shape evolution of metal nanoparticles in water vapor environment. *Nano Lett.* **2016**, *16* (4), 2628–2632.
- (36) Baletto, F.; Ferrando, R.; Fortunelli, A.; Montalenti, F.; Mottet, C. Crossover among structural motifs in transition and noble-metal clusters. *J. Chem. Phys.* **2002**, *116* (9), 3856–3863.
- (37) Baletto, F.; Ferrando, R. Structural properties of nanoclusters: Energetic, thermodynamic, and kinetic effects. *Rev. Mod. Phys.* **2005**, *77* (1), 371.
- (38) Rahm, J. M.; Erhart, P. Beyond Magic Numbers: Atomic Scale Equilibrium Nanoparticle Shapes for Any Size. *Nano Lett.* **2017**, *17* (9), 5775–5781.
- (39) Wang, B.; Liu, M.; Wang, Y.; Chen, X. Structures and energetics of silver and gold nanoparticles. *J. Phys. Chem. C* **2011**, *115* (23), 11374–11381.
- (40) Levitt, M.; Hirshberg, M.; Sharon, R.; Laidig, K. E.; Daggett, V. Calibration and testing of a water model for simulation of the molecular dynamics of proteins and nucleic acids in solution. *J. Phys. Chem. B* **1997**, *101*, 5051–5061.
- (41) Santra, B.; Michaelides, A.; Scheffler, M. Coupled cluster benchmarks of water monomers and dimers extracted from density-functional theory liquid water: the importance of monomer deformations. *J. Chem. Phys.* **2009**, *131*, 124509–1.
- (42) Soper, A. K.; Bruni, F.; Ricci, M. A. Site–site pair correlation functions of water from 25 to 400 °C: Revised analysis of new and old diffraction data. *J. Chem. Phys.* **1997**, *106*, 247.
- (43) Guardia, E.; Skarmoutsos, I.; Masia, M. Hydrogen Bonding and Related Properties in Liquid Water: A Car–Parrinello Molecular Dynamics Simulation Study. *J. Phys. Chem. B* **2015**, *119* (29), 8926–8938.
- (44) Kresse, G.; Hafner, J. Ab initio Molecular Dynamics for Liquid Metals. *Phys. Rev. B: Condens. Matter Mater. Phys.* **1993**, *47*, 558.
- (45) Kresse, G.; Furthmüller, J. Efficiency of Ab-initio Total Energy Calculations for Metals and Semiconductors Using a Plane-wave Basis Set. *Comput. Mater. Sci.* **1996**, *6*, 15–50.
- (46) Kresse, G.; Furthmüller, J. Efficient Iterative Schemes for Ab-initio Total-energy Calculations Using a Plane-wave Basis Set. *Phys. Rev. B: Condens. Matter Mater. Phys.* **1996**, *S4*, 11169.
- (47) Perdew, J. P.; Burke, K.; Ernzerhof, M. Generalized Gradient Approximation Made Simple. *Phys. Rev. Lett.* **1996**, *77*, 3865.
- (48) Grimme, S.; Antony, J.; Ehrlich, S.; Krieg, H. A consistent and accurate ab initio parametrization of density functional dispersion correction (DFT-D) for the 94 elements H–Pu. *J. Chem. Phys.* **2010**, *132*, 154104.
- (49) Kresse, G.; Joubert, D. From Ultrasoft Pseudopotentials to the Projector Augmented-wave Method. *Phys. Rev. B: Condens. Matter Mater. Phys.* **1999**, *59*, 1758.